Current Advances in Optimization of Operative Regimes of Steady State Applied Field MPD Thrusters

IEPC-2019-585

Presented at the 36th International Electric Propulsion Conference
University of Vienna • Vienna, Austria
September 15-20, 2019

A. Boxberger[1], A. Behnke[2] and G. Herdrich[3]
Institute of Space Systems (Institut für Raumfahrtsysteme), University of Stuttgart,
Pfaffenwaldring 29, 70659, Stuttgart, Germany

Abstract: Future interplanetary cargo and manned missions can be performed with chemical propulsion systems at the expense of required propellant, which needs to be launched into the orbit and therefore leading in the long term to a higher transfer costs. High power electric propulsion systems in MW range could enable interplanetary cargo orbit transfers at the expense of increased complexity by offering in a long term a very cost efficient and sustainable transportation via NEP space tugs and ISRU considerations.[1-5] Steady state applied-field magnetoplasmadynamic thrusters (AF-MPDT) are considered of being suitable for high power interplanetary applications in the power range of some MW.[2] This paper presents new results with reviewed setup, improved thrust balance and discharge power levels up to 100 kW with SX3 thruster.[6,7] Additionally, for high voltage operation with anode voltage up to 450 V, a new LaB_6 hollow cathode has been designed for SX3 anode and tested up to the discharge power of 8.6 kW in regulated voltage regime up to 220 V. Finally, a conclusion on further development and perspective evaluation is given with respect to short and long term application of AF-MPD thrusters as a main propulsion system.

I. Introduction

Steady-state Applied-Field Magneto-Plasma-Dynamic Thrusters (AF-MPDT) are very promising for main high power electric propulsion applications[1-5] (e.g. NEP systems) providing an optimal mix of practical trade-offs. The use of gaseous alternative propellants such as argon, ammonia, methane and hydrogen offers ISRU aspects and high potential for propellant costs savings, especially at high power and for long term space infrastructure scenarios. The AF-MPD thrusters feature high power and thrust density, relative high exhaust velocities and therefore are suitable for interplanetary mission scenarios especially in the power range beyond 500 kW.[8] Additionally, by using the configuration of coaxial applied magnetic field coils offers sustainable development towards more advanced hybrid/multistage propulsion concepts in the future. Because of these attributes the AF-MPD thrusters are very promising in the near future for more sustainable and efficient high power applications between 1 and 5 MW, such as automatic cargo transport or manned missions to Mars.[1-4]

State of the art steady state AF-MPD thrusters have demonstrated good performance by reaching thrust efficiencies up to 40 % with argon and up to 50 % with lithium propellant.[8-13] Some references show even higher thrust efficiency than 50 %. However, a careful data analysis is required, especially with respect to ambient pressure requirements below 0.05 Pa.[8,9] Given a high power nature of MPD thrusters and respective high mass flow rates, this is very difficult to achieve on the level of a ground testing facility. There are also still a few major challenges, which need to be addressed and solved in the future.

[1] PhD Student, Institute of Space Systems, adam.boxberger@t-online.de.
[2] PhD Student, Institute of Space Systems, behnke@irs.uni-stuttgart.de.
[3] Head of electric propulsion and plasma wind tunnels, Institute of Space Systems, herdrich@irs.uni-stuttgart.de.

These challenges are:

- Design and scaling criteria
- Applied magnetic field
- Thrust efficiency
- PPU development
- Life time of the cathode
- Passive cooling

Some of these challenges can be solved due to current advances, such as high temperature superconductors (HTS) and high current LaB_6 hollow cathodes.[14-17] Since 1960ies several different AF-MPD thrusters have been developed and tested.[8] However, since AF-MPDT concept can cover different operational regimes and acceleration mechanisms[8,18,19] (from thermal to electrostatic), it is not clear yet which operational regimes would be the most promising solution for high power applications. The main regimes of an AF-MPD thruster can be categorized in following 3 groups[18,19] (thermal acceleration excluded):

1. **Self induced field centric acceleration** with low voltage operation (~ 40-80 V) and high discharge current with a relatively weak applied magnetic field (~ 0.1 T)[11-13,20]
2. **Swirl centric acceleration** with high voltage operation (~ 120-170 V) in a strong applied magnetic field (> 0.2 T) and with a moderate discharge current[6,9,21-23]
3. **Hall-effect centric acceleration** with high voltage operation (> 200 V) and low discharge current in a very strong applied magnetic field (> 0.4 T) (potentially hybrid mode of 2 and 3, presented in this paper)

However, in operation of an AF-MPD thruster a mix of two or three acceleration mechanisms can occur depending on geometry and operational conditions. A more detailed breakdown of acceleration mechanism was given by Sasoh et al..[18] With different acceleration mechanisms a more refined optimization in hardware would be required for an application leading to a different complexity and costs. The experimental results presented in this paper show investigations of SX3 thruster mainly oriented towards swirl and Hall-effect centric acceleration regimes.

II. Experimental Setup

A. Testing Facility

The results presented in this paper have been performed in MPD testing facility Tank 8 (IRS laboratory), which has been adapted for higher power operation in steady state regime close to 100 kW discharge power in strong magnetic field of 400 mT. The thruster and thrust balance assembly are implemented in stainless steel water cooled vacuum chamber with dimension of ⌀ 2×5 m. The inside surface of the vacuum chamber was coated with ceramic coating in plume downstream region in order to prevent discharge interaction with vacuum chamber. The central vacuum facility can provide a total throughput of more than 250 000 $m^3 \cdot h^{-1}$ at approximately 1 Pa and a minimal achievable pressure of ~ 0.4 Pa at argon mass flow rate of ~ 30 mg/s. However, according to the literature the required ambient pressure for operation of AF-MPD thrusters is below 0.05 Pa, which is lower compared to presented results. The high power DC facility can provide 2 separate current controlled circuits, which can be adjusted in the range of 2.5 and 1 kA with up to 1 kV each for operation of an AF-MPD thruster. Additional power supplies have been used for LaB_6 hollow cathode tests with 460V - 40A (voltage controlled) for the main anode discharge, 115V - 40A for the heater, and 300V - 10A (voltage or current regulated) for the keeper. All power supplies are potential free.

For the cooling purpose high pressure pumps with closed water cycle of the central cooling facility can provide up to 25 bar cooling water distributed in 4 cooling circuits: anode, coil, thruster assembly, and setup parts, with theoretical cooling power of ~ 300 kW. The data acquisition system with a measuring program has an average measuring frequency of 10 Hz. Monitoring of the vacuum pressure is done by two Pfeiffer PKR 251 wide range pressure gauges placed on opposite ends of the vacuum chamber. Current measurements are performed by measuring drop voltage on predefined shunts on both circuits via galvanic isolation amplifier (on "–"and "+" side). Structural and water temperatures are monitored by PT100 resistance thermometers (Class A and 1/3 DIN). Cooling water mass flow rates of respective parts were measured in air conditions with non-operational thruster and without thermal load by using magnetic-inductive water mass flow meters (SIEMENS MAG 1100 DN6). The anode and cathode propellant distribution is provided by a two pairs of Bronkhorst F-201CV type flow controllers with up to 10 and 100 $mg \cdot s^{-1}$ of argon.

B. Thrust Balance

For the purpose of thrust measurements, the MPD test stand includes a parallelogram pendulum thrust balance, which is connected via fixed frame with the vacuum chamber's tank lid (see Fig.1 and Fig.2). The current supply decoupling of the balance assembly was realized with flexible wire strand made out of copper filaments (75mm² each). In the case of cooling water channels, the tubes (Polyamide, Ø12×1.5) were mounted and fixed in a half circle shape perpendicular to the thruster's axis in order to minimize spring like loads of the tubes. Thrust acquisition has been done with the S-shaped force sensor (KD40s) with a nominal measuring force of 5 N and base accuracy of ± 5 mN. The force sensor can be moved on a linear unit towards the balance allowing a desired preload force or decoupling from thrust balance completely. In order to characterize the measured force sensor signal a calibration unit is implemented with 3 weights representing a reference force of 2.837 N in total. For calibration the weights apply a force in the thrust direction via thin Dyneema® line and two precision lube free pulleys. The KD40s sensor was calibrated before implementation by applying vertical load with same calibration masses (for reference purpose). Additionally, an inductive distance sensor multiNCDT 300 S1 with a measuring range of 1 mm and resolution of 0.1 µm has been implemented for characterization of the pendulum and potential null balance design setup.

The thrust balance was characterized in a fully assembled setup (thruster included) by measuring preload and displacement of the balance. Figure 3 shows the thrust balance characteristic at different preloads and added calibration weights and respective change in inclination. Loads like calibration masses, thrust, cold gas act against the force sensor leading to deflection change - dθ, whereas negative tare forces act in the opposite direction and respective + dθ change. These changes are considered in calibration, evaluation of tare forces and thrust via data post processing (equal to direct thrust measurements with null balance design).

The thrust measurements performed back in 2016 were performed with relatively low frequency (~ 10Hz) of the main data acquisition system.[6,24] The thrust measurement was affected by low time resolution and oscillations caused by high pressure water cooling and respective pressure variations through 64 pipes connected to the pendulum. In order to improve the quality of the measurements a digital oscilloscope LeCroy 24Xs has been used for force and distance sensor. The sampling rate and acquisition time have been adjusted to 10 µs per point and 5 seconds in total. The acquired data was automatically post processed by creating mean data points of force and distance sensor for respective operation conditions. Synchronization of thrust and operative data was done via manual time tags with an average deviation up to 5 seconds. An exemplary set of force sensor data (exp. series 202) is shown in Fig. 4, where the discharge current was increased from base level of 200 A to the maximum of 575 A. During these measurements the B-field and mass flow rate were kept constant. Overall the thrust can be measured with an accuracy of ca. ± 140 mN. An exemplary cold thrust data is presented in III E section (no cooling water).

Due to limitations of cooling facility especially while operating in 400 mT conditions a steady drift of inlet water temperature has been observed during review of 2016 test campaign.[6,24] This leads to a drift of the force sensor signal and reduction of reliable thrust data to pre-shutdown conditions only. This affects mostly all set of data from 2016 test campaign.[6,24] In order to maximize data output, a reference condition is measured in series of conditions at the beginning and at the end (before shut down of the thruster), allowing an evaluation of drift slope and recalibration of data under assumption of constant thermal drift (see Fig.2). Therefore, a specific base condition should be matching before and after in discharge characteristic. During the whole series of measurement the B-field and mass flow rate are constant, while discharge current / voltage might be varied. For the final thrust values tare forces and cold gas need to be added in a post processing analysis. However, since the magnitude of the cold gas thrust is close to the accuracy of the thrust balance, therefore the presented data do not include cold gas portion of thrust.

Overall the new test procedures significantly improve the quality and reliability of the thrust measurements, which additionally are covered by evaluation of heat losses (see result section). A more detailed overview of the thrust balance is given in a extra reference.[7]

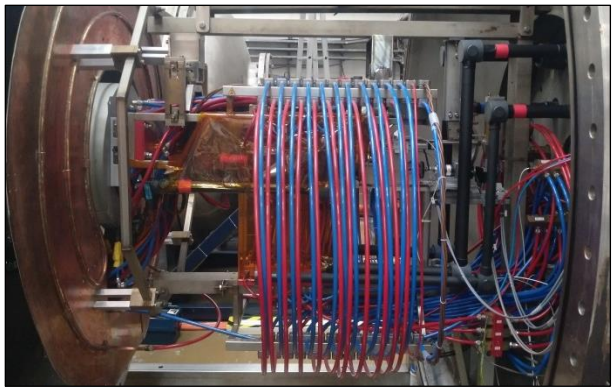

Figure 1. Thrust balance assembly with mounted heat shield and thruster assembly.

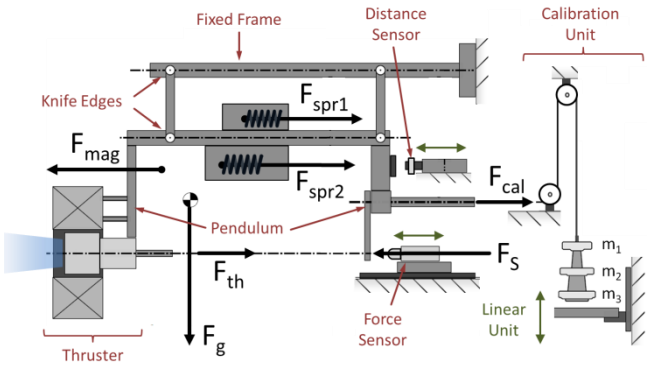

Figure 2. Schematic overview of parallelogram thrust balance.

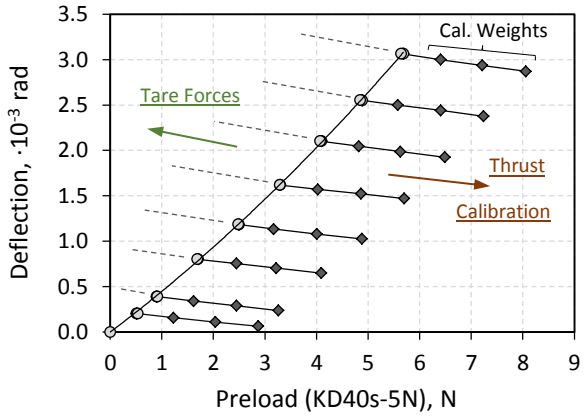

Figure 3. Preload of the force sensor and respective deflection characteristic of the pendulum (thruster, decoupling of water/power supply are included).

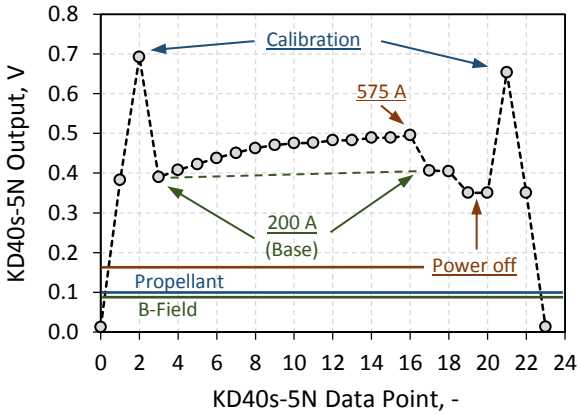

Figure 4. Output mean data set of measured series for the force sensor, experiment 202 (200-575A, 60mgs argon and 100mT).

C. Thruster

The 100 kW steady-state AF-MPD thruster SX3 was designed as costs effective water cooled laboratory model (shown in Fig.5 and Fig.6). The anode assembly is made out of copper and the hollow cathode made out of thoriated tungsten rod (WT20), which is EB welded on respective copper mounting adapter. All insulators in discharge proximity (anode liner and cathode centering) are made out of boron nitride. Other insulation parts were realized with alumina, steatit, MACOR, PEEK or PVC. The thruster has a modular design allowing a potential implementation of different electrodes. The electrode ratio with ø 12/6 mm hollow cathode is about 7.167 and is relatively high compared to other applied-field MPD thrusters.[8-13] Other electrode ratios of 14.333 and 3.583 are already manufactured and will be tested in the near future (ø 6/3 mm and ø 24/12 mm respectively). This will allow an extension of experimental data towards high current or voltage regime. Before each implementation procedure into experimental setup the thruster assembly has been checked for potential gas and water leakages. An additional heat shield between applied-field coil and thruster protects cooling water and gas supply PA pipes.

The assembly of applied magnetic field coil has dimensions of D500 / d325 mm and is 145 mm long. The total amount of coil turns is about 71, which are implemented via soft copper pipes (15 m, ø 10x1 mm). The implemented assembly of SX3 thruster and SX coil is shown in Fig.6. The characterization of the coil was performed in previous work.[6] A typical operative range of the coil is between 235 and 1880 A with the slope of 50 mT per 235 A. The coil allows a maximum applied magnetic field of 400 mT at electric power of ca. 285 kW. However, the power of applied-field coil is not included in the evaluation of the thrust efficiency. This is justified by consideration of HTSC (high temperature superconductor coil) in high power application case (e.g. +500 kW).

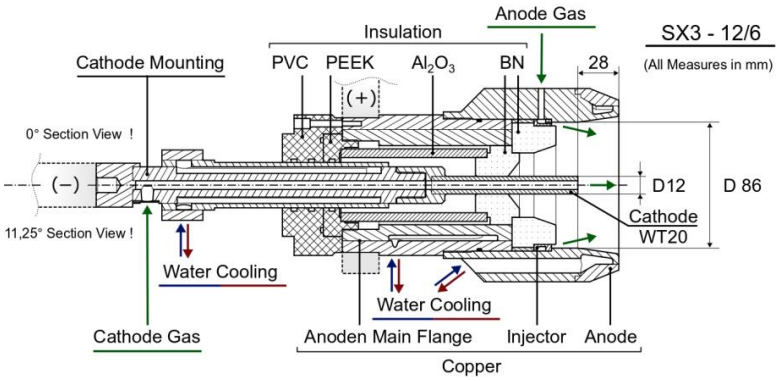

Figure 5. Sectional view of SX3 thruster with ⌀ 12/6 mm WT20 single channel hollow cathode.

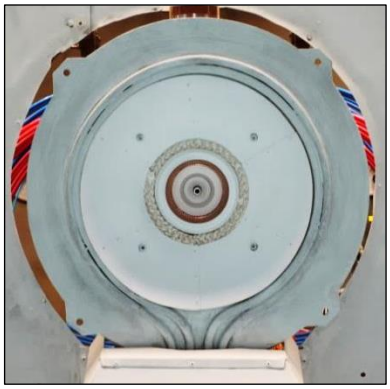

Figure 6. SX3 thruster and SX coil assembly integrated into setup.

D. LaB_6 Hollow Cathode

With increasing demand of high power EP systems and increasing power of Hall-effect thrusters e.g. X-3[25,26] and therefore respective current levels of hollow cathodes the new advances in lanthanum hexaboride (LaB_6) hollow cathodes (see Goebel et al.[15]) seem to be very promising. The benefits apply not only to Hall thrusters, but also to MPD thrusters operated at relatively high voltages. First attempts in operation of LaB_6 cathodes in MPD devices have been performed in Nagoya[19,22,23] and Princeton University[27]. In order to test the feasibility and operation in high voltage mode a new laboratory type LaB_6 hollow cathode with nominal current of < 40 A has been design, manufactured and tested (see Fig.7 left and center image). Most parts are modular allowing replacement and modifications e.g. extension to higher current levels, different orifice diameter or implementation of diagnostics.

In the current configuration the surface area of LaB_6 emitter is about 1.9 cm². The emitter cylinder is fixed in position by graphite sleeve and pusher rod. The cathode front orifice is about 5 mm in diameter and made out of WLA10. The keeper has exchangeable orifice plate with inner diameter of 5 mm. Due to the water cooled design of the anode assembly a relatively high thermal leakage can be expected. Nevertheless, the heating power of < 440 W is sufficient to ignite the cathode in the range of 150 V. After ignition of the keeper discharge the heater is powered down and switched off completely (then switched to floating). Figure 7 (right) shows keeper discharge in operation at 8 A and 1 mg/s of argon.

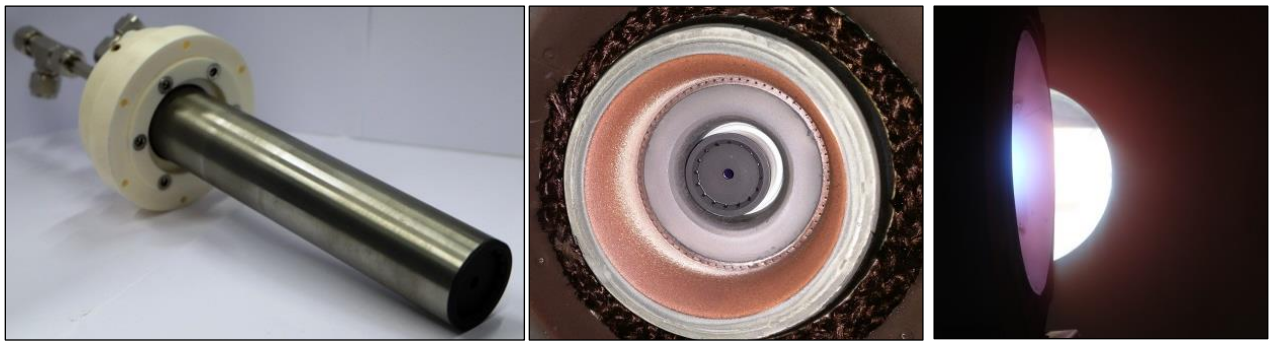

Figure 7. LaB_6 hollow cathode assembly thruster flange not included (left), integrated into assembly of the thruster (center), and in operation with 8 A of keeper current, 1 mg/s of argon and heater off (right side).

III. Experimental Results

E. Tare Forces and Cold Gas Measurements

The characterization of tare forces has been performed in vacuum conditions of 1 Pa. Both electrode interlinks have been tested (25 and 150 mm), in order to simulate different extension of discharge current. Due to the unknown nature of diffuse discharge extension and very small difference of the results between two interlinks, only the 150 mm results of tare forces have been used for evaluation of thrust (see Fig.8). The evaluated tare forces scale with ca. $-3.73 \cdot 10^{-3}$ N/(AT). However, no tare forces have been characterized with the new power supply lines for the LaB_6 hollow cathode. By comparing new tare forces with results presented in 2017[6] a significant improvement in quality and consistency of thrust measurements can be observed.

These improvements can be also seen in the cold thrust measurements (see Fig.9) without cooling water, whereas in previous campaign cold gas measurements were spread without any relevant trend. Figure 9 shows argon results of series measurement in 15 mg/s increments and 50/50 % mass flow rate distribution between the cathode and the anode, and on/off measurements with ca. 90 s long intervals for on and off period of mass flow meters respectively. Below 30 mg/s no obvious trend could be observed. However, cold gas thrust was not included in evaluation of total thrust in any of presented results, since the cold gas fraction is comparably low (0.4-2 %).

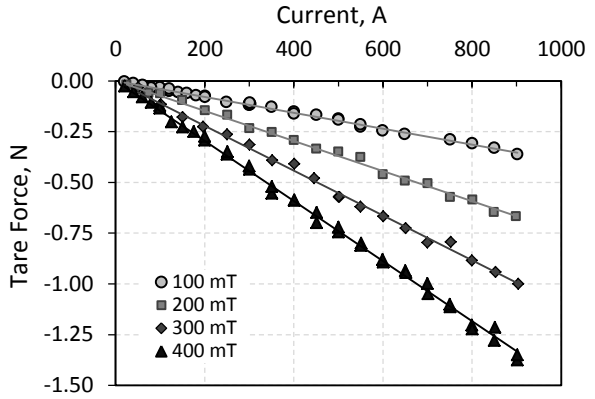

Figure 8. Characteristics of electromagnetic tare forces with 150 mm electrode interlink at respective applied magnetic fields (regulated current setup).

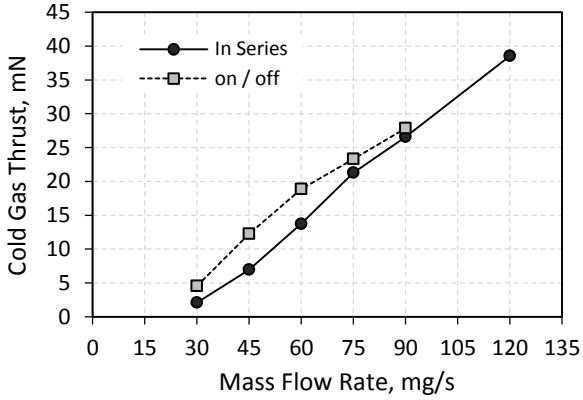

Figure 9. Argon cold gas thrust with 50/50 mass flow rate distribution (no cooling water).

F. Variation of Ambient Pressure

According to literature the vacuum or ambient pressure is the most critical factor for an operation of steady state AF-MPD thrusters. Therefore, additional effort was put into characterization of preselected conditions at different vacuum chamber pressures. Both test conditions were operated with 10+20 mg/s of argon (cathode + anode), with discharge current of 150/300 A and 150/250 A, and applied magnetic field of 100 and 400 mT respectively. The ambient pressure was measured at two different locations, behind the thruster (upstream, probe p_1) and further plume downstream behind the heat shield target (probe p_2). The presented results of probe 2 consist of separate measurements on different days (mainly between 0.24 and 0.7 Pa) with complementation of single measurement series at higher pressures above 0.35 Pa via vacuum system bypass flow (air).

Figures 10-17 show pressure dependence of discharge voltage, thrust, thrust efficiency and anode heat power fraction for 100 and 400 mT. Figure 18 shows thrust per discharge current unity as a function of ambient pressure (p_2) for comparison purpose with X13 and X9 thruster from DFVLR.[9] The difference between p_1 and p_2 (shown in Fig.19) is proportional to p_2. This effect is stronger at higher discharge current and caused by re-entrainment of the ambient into extended discharge volume.

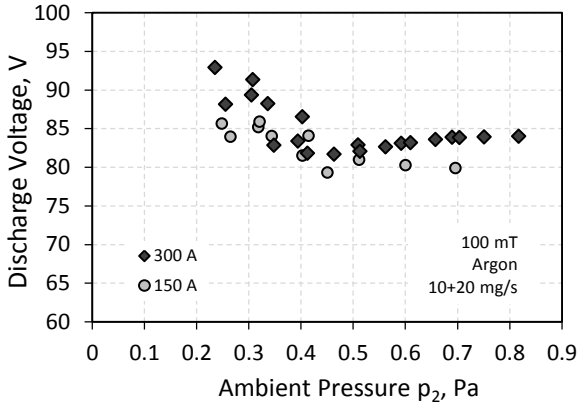

Figure 10. Discharge voltage at respective ambient pressure (p_2, 10+20 mg/s and 100 mT).

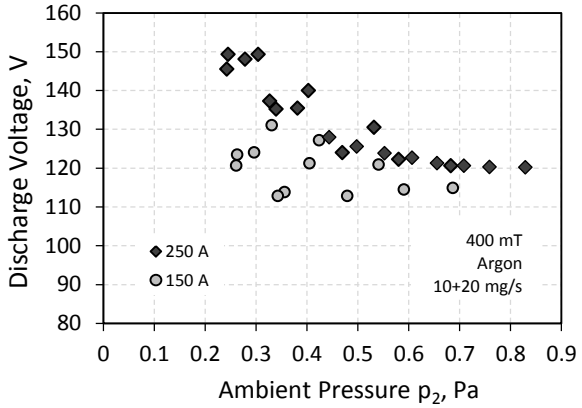

Figure 11. Discharge voltage at respective ambient pressure (p_2, 10+20 mg/s and 400 mT).

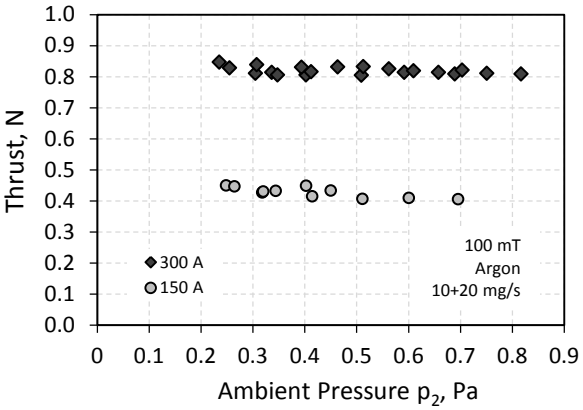

Figure 12. Thrust at respective ambient pressure (p_2, 10+20 mg/s and 100 mT).

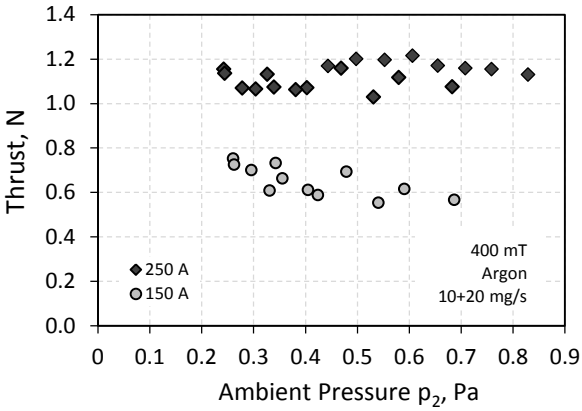

Figure 13. Thrust at respective ambient pressure (p_2, 10+20 mg/s and 400 mT).

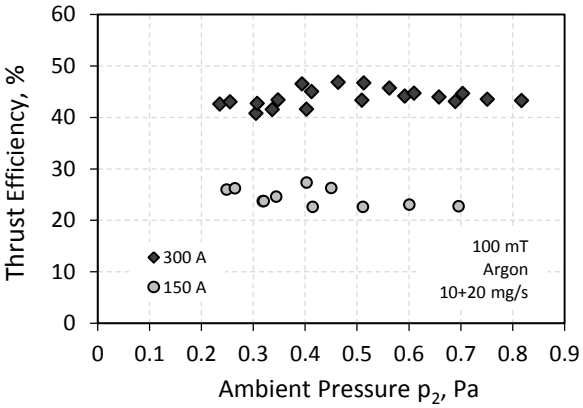

Figure 14. Thrust efficiency at respective ambient pressure (p_2, 10+20 mg/s and 100 mT).

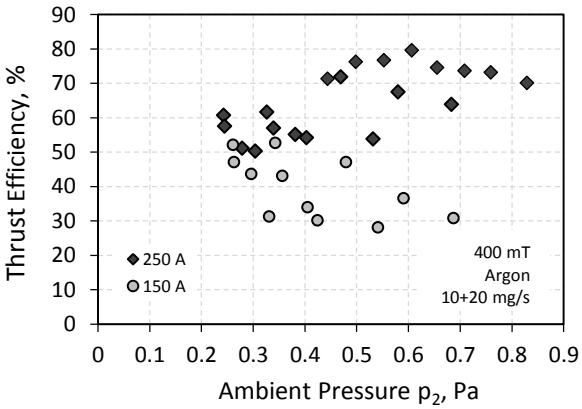

Figure 15. Thrust efficiency at respective ambient pressure (p_2, 10+20 mg/s and 400 mT).

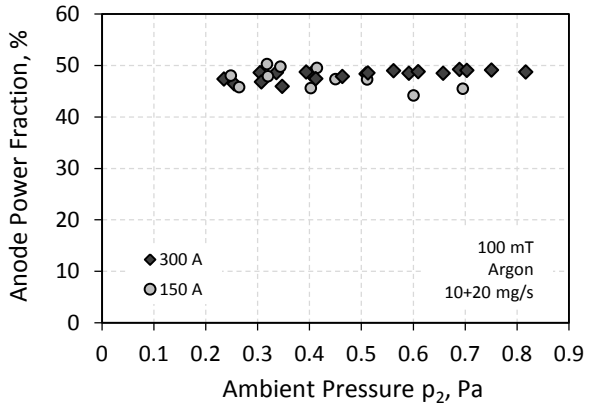

Figure 16. Anode heat power fraction at respective ambient pressure (p_2, 10+20 mg/s and 100 mT).

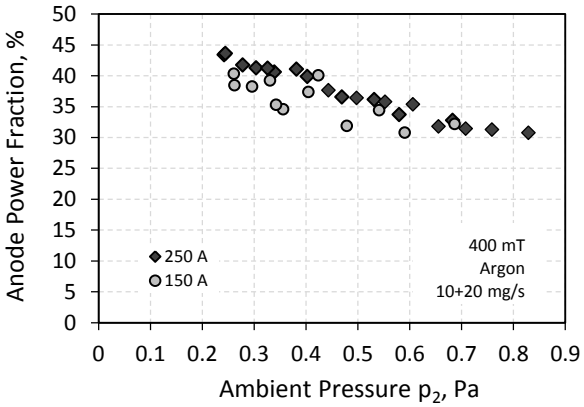

Figure 17. Anode heat power fraction at respective ambient pressure (p_2, 10+20 mg/s and 400 mT).

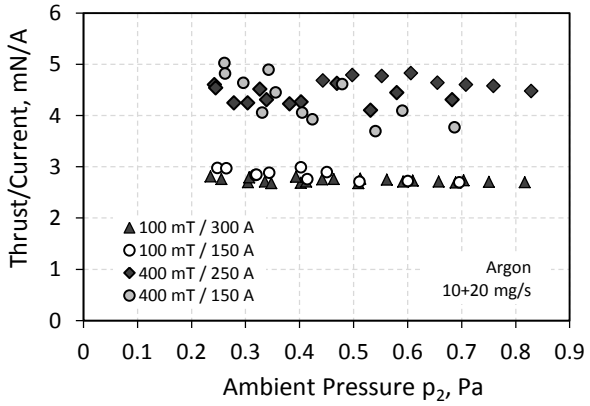

Figure 18. Thrust/current in mN/A as a function of ambient pressure (10+20 mg/s).

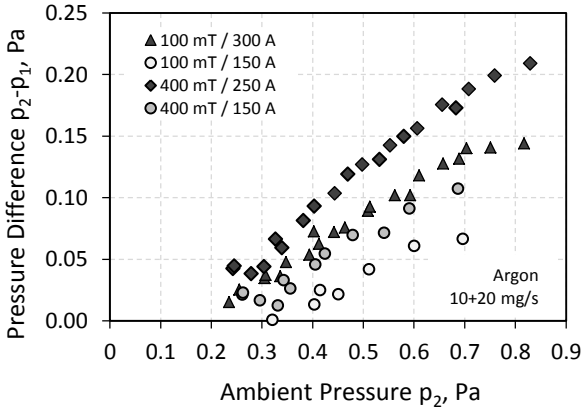

Figure 19. Pressure difference between probe 1 and probe 2 as a function of p_2 (10+20 mg/s).

The results show a significant influence of ambient pressure on the discharge voltage for both cases (100 and 400 mT, shown in Fig.10 and 11). However, the pressure dependency of the thrust is less dominant (Fig.12 and 13), which is also reflected in the thrust per current unity as a function of pressure (Fig.18) with almost no dependency, whereas in case of X13 and X16 thrusters thrust/current increases towards lower pressure.[9] As a consequence the thrust efficiency change is mainly influenced by the discharge voltage increase towards lower pressures, indicating a further efficiency drop below 0.1 Pa down to 40 % (especially in case of 400 mT conditions at 250 A). This would lead to similar thrust efficiency as in the case of X16 thruster with ca. 38 % indicating the importance of ambient pressure requirements below 0.05 Pa, as recommended in multiple references.[8,9] The anode heat power fraction of all 100 mT conditions seems to be less affected by the ambient pressure than at 400 mT. Overall it can be concluded that for steady state operation of swirl centric AF-MPD thrusters a lower ambient pressure is required compared to self-field centric thrusters, whereas Hall centric or hybrid AF-MPDTs might have similar ambient pressure requirements as in case of Hall-effect or TAL thrusters.

G. Integral Measurements and Performance

For optimization purpose the SX3 thruster has been characterized at 100, 200 and 400 mT of applied magnetic field, and with anode mass flow rate ratio of 25, 50 and 75 %. The discharge current has been varied up to 350 A. High voltage operation mode with discharge voltage in range of 200-240 V was specifically triggered in regulated discharge current operation.

Figures 20-22 show the discharge characteristic and Fig. 29-31 show anode heat power fraction for respective mass flow rate ratio (cathode/anode in %). The performance of the thruster is shown in Fig. 23-28 and in Fig. 32-34 showing thrust, thrust efficiency and specific impulse.

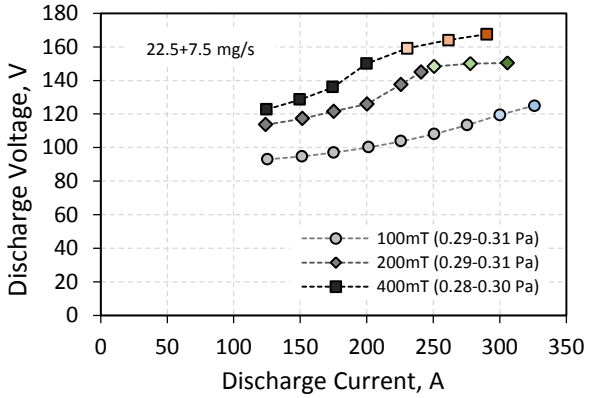

Figure 20. Discharge characteristic with 75/25 % mass flow rate distribution.

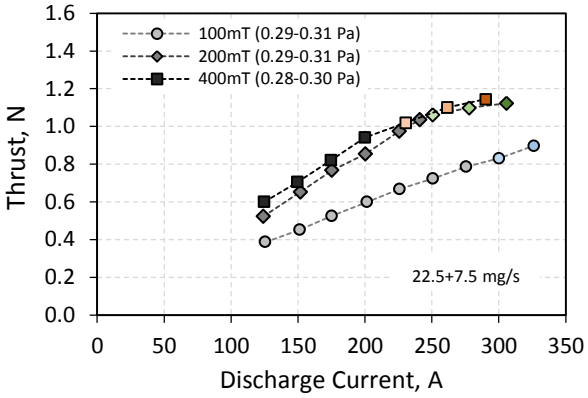

Figure 23. Thrust as a function of discharge current with 75/25 % mass flow rate distribution.

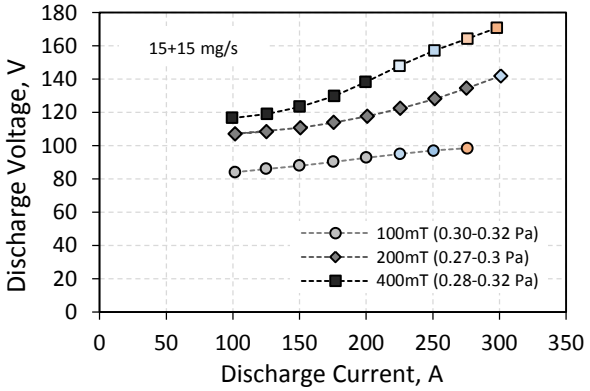

Figure 21. Discharge characteristic with 50/50 % mass flow rate distribution.

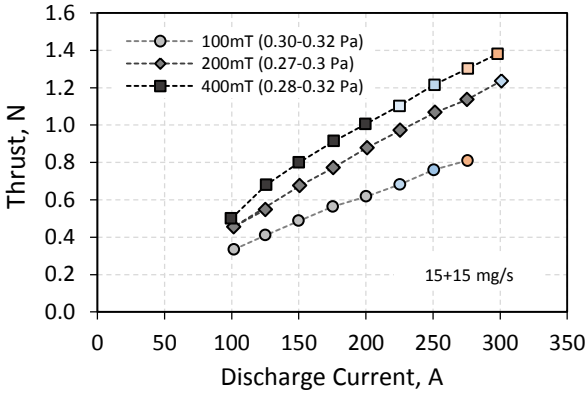

Figure 24. Thrust as a function of discharge current with 50/50 % mass flow rate distribution.

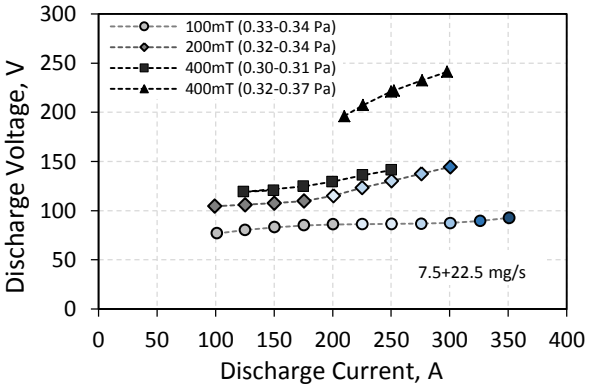

Figure 22. Discharge characteristic with 25/75 % mass flow rate distribution.

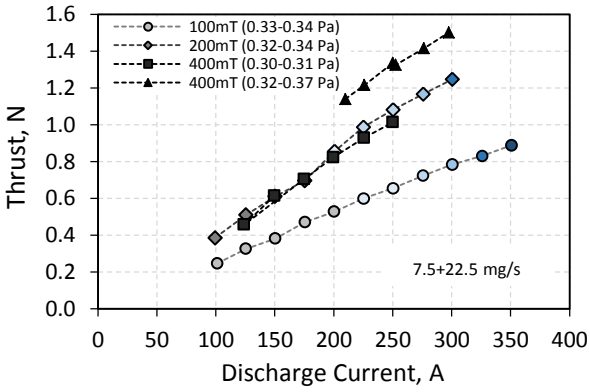

Figure 25. Thrust as a function of discharge current with 25/75 % mass flow rate distribution.

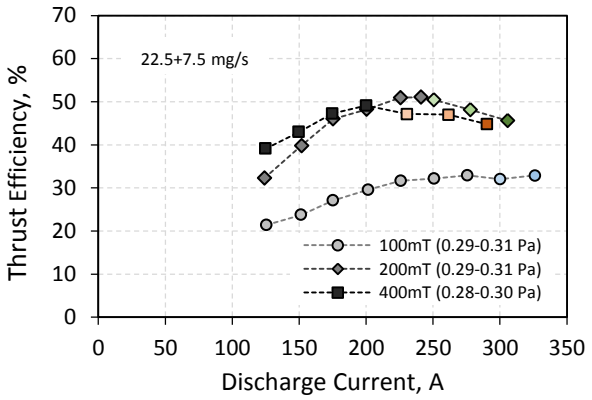

Figure 26. Thrust efficiency as a function of discharge current with 75/25 % mass flow rate distribution.

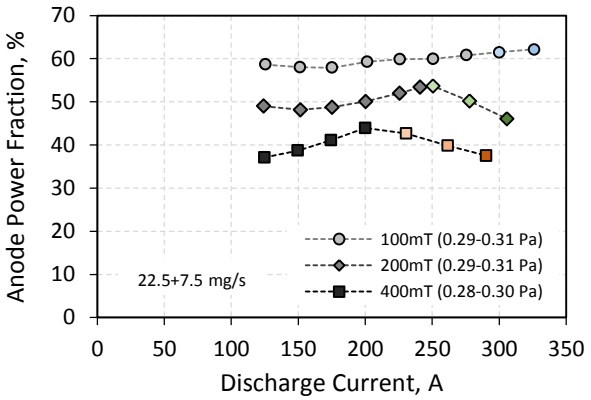

Figure 29. Anode heat power fraction with 25/75 % mass flow rate distribution.

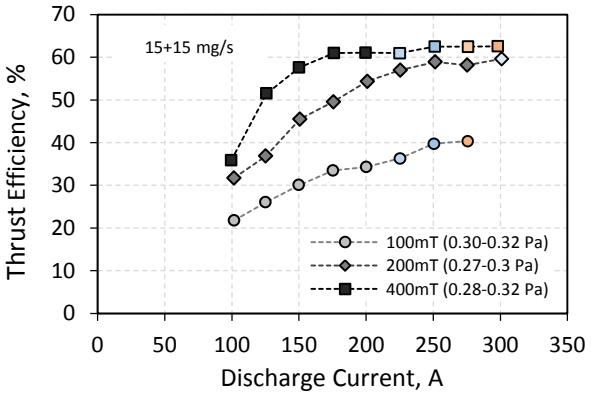

Figure 27. Thrust efficiency as a function of discharge current with 50/50 % mass flow rate distribution.

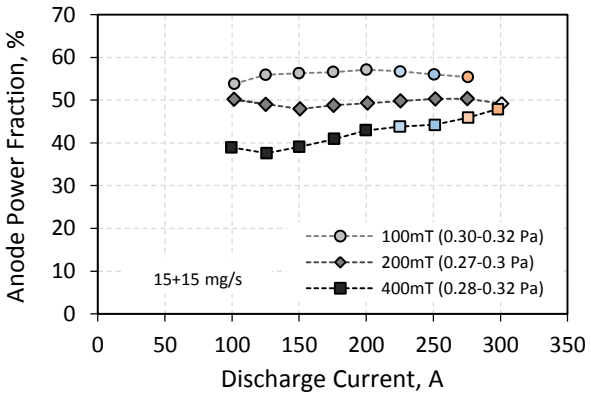

Figure 30. Anode heat power fraction with 50/50 % mass flow rate distribution.

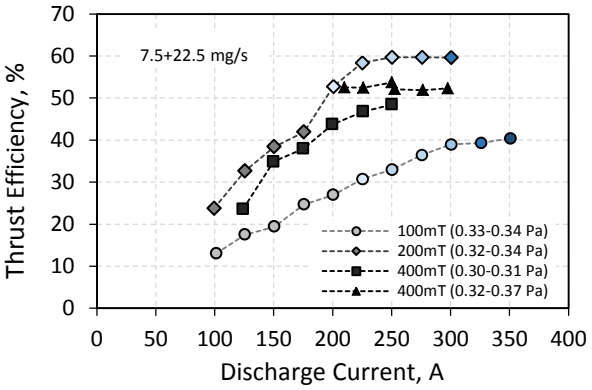

Figure 28. Thrust efficiency as a function of discharge current with 25/75 % mass flow rate distribution.

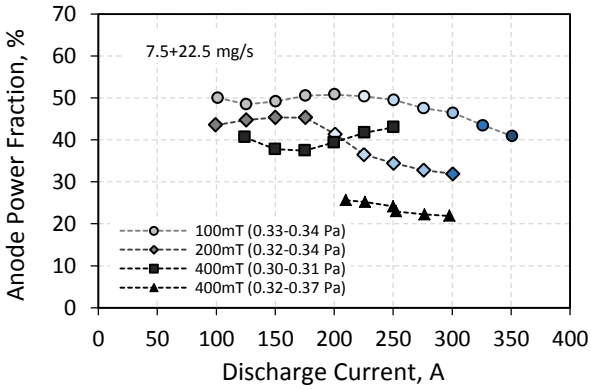

Figure 31. Anode heat power fraction with 25/75 % mass flow rate distribution.

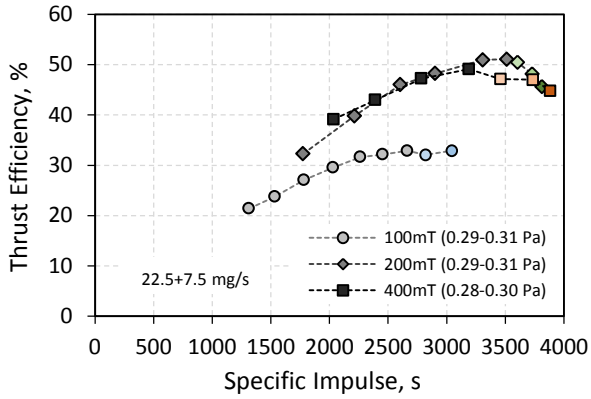

Figure 32. Thrust efficiency as a function of specific impulse for 75/25 % mass flow rate distribution.

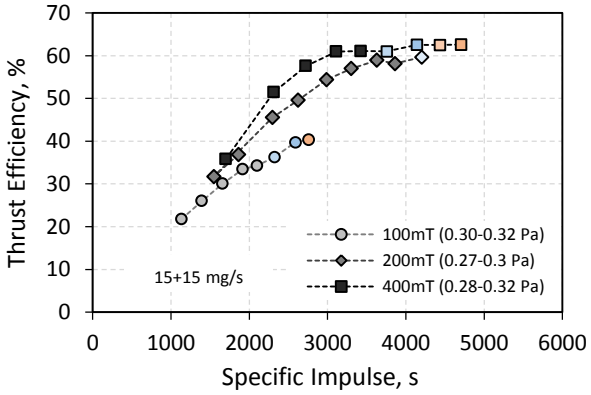

Figure 33. Thrust efficiency as a function of specific impulse for 50/50 % mass flow rate distribution.

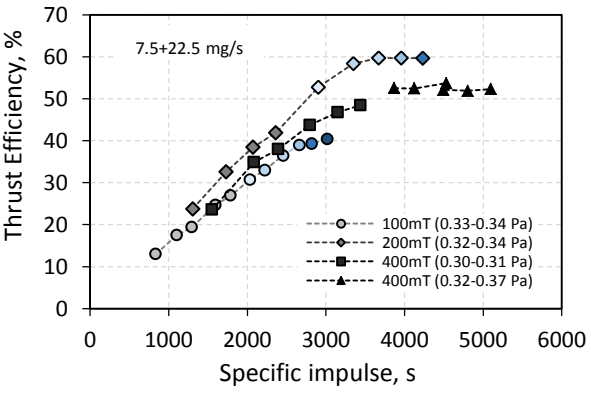

Figure 34. Thrust efficiency as a function of specific impulse for 25/75 % mass flow rate distribution.

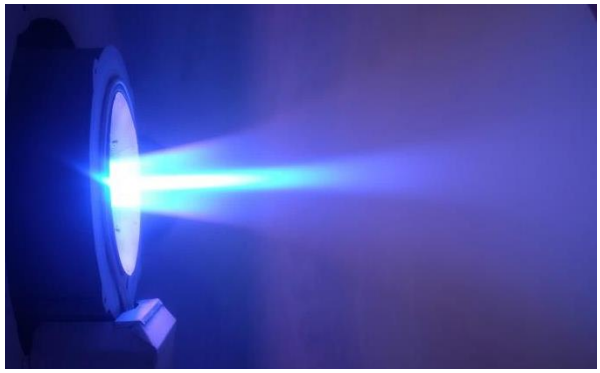

Figure 35. Argon plume with 50/50 mass flow rate distribution, 250 A, 97 V, 30 mg/s and 100 mT.

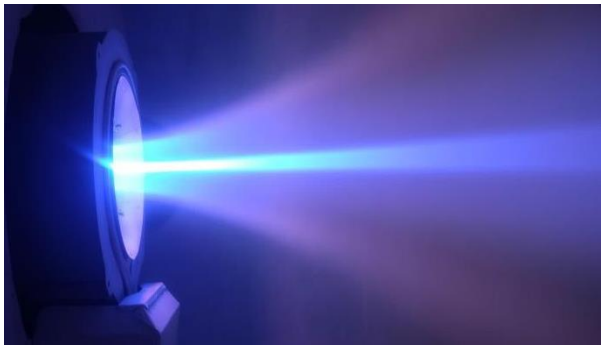

Figure 36. Argon plume with 50/50 mass flow rate distribution, 250 A, 157 V, 30 mg/s and 400 mT.

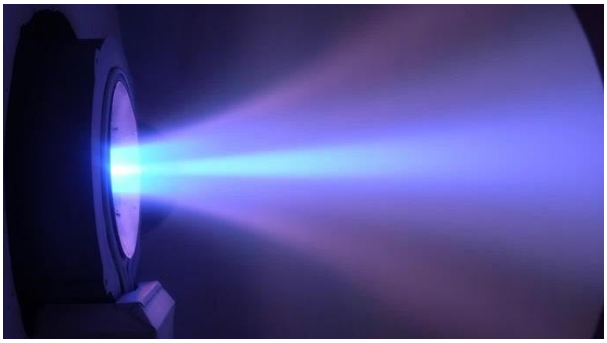

Figure 37. Argon plume with 25/75 mass flow rate distribution, 250 A, 220 V, 30 mg/s and 400 mT.

All plots with orange marked conditions had increasing discharge voltage oscillations and widening of the cathode plume. Green conditions were operated with oscillations in the discharge characteristic and blue points with widening of the plume only. The difference in plume appearance between different operational modes is shown in Fig.35-37, showing self-field, swirl and hybrid (Hall + swirl) centric acceleration regimes. As indicated by blue dots

in 50/50 plots, the cathode plume is flared towards vacuum chamber / heat shield target (Fig.35, 36). This effect is very dominant in 25/75 100 mT conditions with the discharge current levels of more than 200 A. This might be caused by vacuum chamber interaction or to high ambient pressure or the combination of both. A change in the discharge characteristic (U-I slope) and in anode heat power fraction is likely an additional indicator for and ambient or a chamber interaction. A local increase of multiple charges could be also a potential explanation. However, in vacuum conditions below 0.05 Pa and preferably bigger vacuum chamber all colored conditions could be in unstable regime, including discharge voltage oscillations, plume fluctuations or even onset. This needs to be considered in evaluation of the performance of presented results, especially under consideration of section III F in this paper. In following discussion all colored points are neglected.

At 100 mT the best performance is achieved with 75/25 and 50/50 mass flow rate distribution. In case of 200 mT conditions best performance was achieved with 50/50 mass flow rate distribution and 250 A, with a thrust of 1.07 N (33 mN/kW), 3630 s and thrust efficiency of 58.9 %. Even without widening of the plume or discharge oscillations, this condition seems to over perform, especially regarding the anode heat power fraction of 50.3 %. At strong magnetic field of 400 mT, the highest efficiency of 60.9 % was reached with 50/50 mass flow rate distribution and anode heat power fraction of 40.9 %. Due to a very strong extension of the discharge current, swirl centric acceleration seems to be most affected by the ambient gas. Specifically triggered high voltage mode operation with 25/75 mass flow rate distribution has achieved a maximum thrust efficiency of ca. 52 %. Because of very high specific energy of 2.39 kJ/kg, the estimated *Isp* is about 5097 s, which is comparably high, but seems to be reasonable considering 71.82 kW of discharge power. This condition not only has the highest discharge power and specific impulse but also the highest thrust of 1.5 N. The anode heat power fraction shows a decreasing behavior with stronger applied magnetic field and drops significantly in high voltage regime down to 25-20 %. However, a potential error in the measurement cannot be excluded, since the measurement of the anode temperature and therefore of d*T* at given power level is in a range of 1 K (± 0.2 K accuracy), due to a relatively high mass flow rate of cooling water. Additionally, a not expected temperature offset was observed in some of the measurements especially in very unstable regimes. Nevertheless, the presented results at medium power levels are very promising, but would require an additional assessment especially under consideration of lower vacuum chamber pressure.

H. Exemplary Results of High Power Conditions

The results presented in this paper represent only a fraction of performed test campaign. Different mass flow rates and mass flow rate ratios have been tested up to discharge power of 100 kW. Table 1 shows an overview of selected conditions for different operational modes, such as self-field centric acceleration in column 1, swirl centric mode in column 2 and 3 and hybrid /Hall centric acceleration in column 4 with high voltage operation. The author places emphasis on importance of ambient pressure dependency for evaluation of the results. A respective plume representation of each mode is shown in Fig.38-41.

Table 1. High power conditions up to 100 kW of discharge power at different applied magnetic fields.

Experiment Nr.	216	228	214	227	217	229	149	231
Applied Field, mT	103	103	203	202	402	401	403	402
Discharge Power, kW	74.81	70.28	102.74	100.44	99.85	100.81	49.48	101.52
Discharge Current, A	750.6	769.6	700.1	728.1	586.5	623.7	222.6	441.0
Discharge Voltage, V	99.7	91.3	146.7	137.9	170.2	161.6	222.3	230.2
Mass Flow Rate, mg/s	90.00	120.07	90.09	120.09	90.08	120.07	30.06	60.10
Ambient Pressure p2, Pa	0.43	0.50	0.44	0.50	0.38	0.46	0.32	0.40
Anode Power Fraction, %	44.88	42.79	43.27	41.81	40.58	37.98	17.77	24.10
Specific Energy, kJ/kg	0.83	0.59	1.14	0.84	1.11	0.84	1.65	1.69
Thrust, N	2.09	2.27	2.72	2.99	3.21	3.59	1.10	2.75
Thrust/Power, mN/kW	27.98	32.25	26.51	29.72	32.17	35.61	22.28	27.09
Specific Impulse, s	2371	1924	3082	2534	3635	3048	3738	4665
Thrust Efficiency, %	32.53	30.44	40.09	36.95	57.35	53.23	40.85	61.99

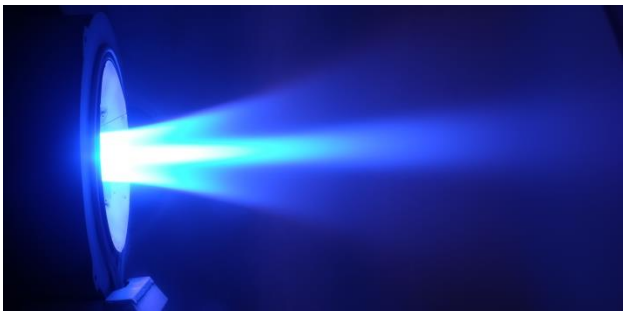

Figure 38. Plume appearance at 100 kW of discharge power, 120 mg/s of argon and 200 mT (exp. 227).

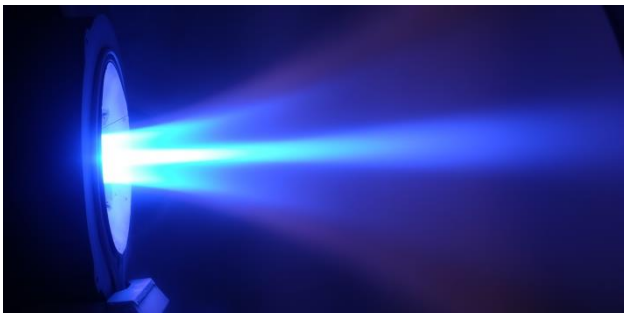

Figure 39. Plume appearance at 100 kW of discharge power, 120 mg/s of argon and 400 mT (exp. 229).

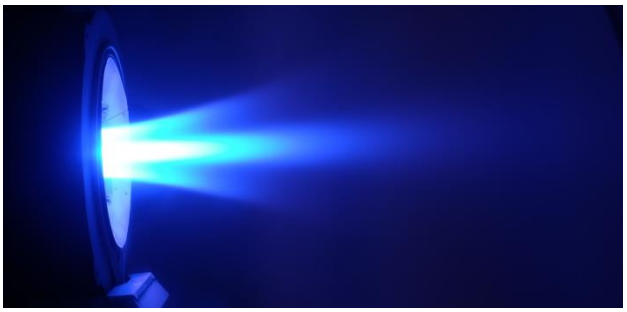

Figure 40. Plume appearance at 70 kW of discharge power, 120 mg/s of argon and 100 mT (exp. 228).

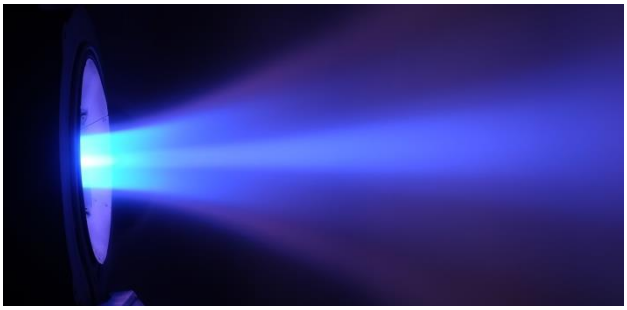

Figure 41. Plume appearance at 100 kW of discharge power in high voltage regime, 60 mg/s of argon and 400 mT (exp. 231).

The difference between operational modes can be seen in the plume appearance, discharge voltage and specific energy at which the thruster provides the best performance. In case of 100 mT conditions higher mass flow rates will be required for 100 kW conditions. Therefore, it is very difficult to compare all three modes in one thruster geometry, due to different design requirements. As a consequence this leads to further optimization process of the hardware for desired operation. In SX3 thruster this can be achieved via different cathode geometries (electrode ratios) and mass flow rates. Overall considering the vacuum capability of the facility the most promising approach would be the self-field centric operation at 100 mT and mass flow rate between 100 and 200 mg/s (argon). Nevertheless, from scientific point of view proof of concept experiments are also important such as LaB_6 hollow cathode test shown in the next section. The SX3 thruster has been operated for more than 41 hours with WT20 12/6 hollow cathode (regulated current). With the estimated amount of charge of ca. $3.682 \cdot 10^7$ C and mass loss of 45.071 g (in 2 campaign) the effective erosion rate of the cathode is about 1.22 ng/C.

I. Operation with LaB6 Hollow Cathode and Regulated Voltage

The application of LaB_6 emitter seems to be very promising[15] and with some adaptations could be used in MPD thrusters. However, due to the limited experience of LaB_6 hollow cathodes in a B-field environment with more than 100 mT, initial proof of concept experiments have been performed with LaB_6 hollow cathode (see section II D) with regulated voltage power supply (450V and 40 A).

The cathode is ignited at ca. 440 W power of the heater and 160 V of keeper voltage. Then the heater is turned off and applied magnetic field is set to specific condition of anode discharge. Figure 42 and Fig.43 show the keeper discharge in operation at 100 and 400 mT respectively. Some preliminary experiments have been performed with anode discharge and keeper in operation at 2.5 A. However, multiple tests have been also performed without keeper and anode discharge only. Figure 40 shows preliminary proof of concept results at different anode voltage levels in range of 100-225 V. Considering the geometry of SX3 thruster and given mass flow rates the discharge characteristic is similar to the experiments performed at Nagoya University.[19,22,23] Figure 41 shows the plume difference between 150 and 220 V of anode voltage operation at 200 and 400 mT respectively, which is similar to the difference between plume in Fig.38 and Fig.41 in regulated current operation with WT20 12/6 cathode.

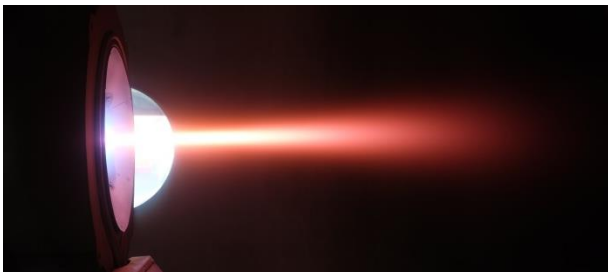

Figure 42. Keeper discharge with 10 A and 100 mT (heater off).

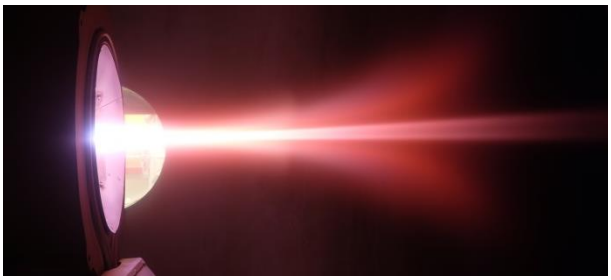

Figure 43. Keeper discharge with 10 A and 400 mT (heater off).

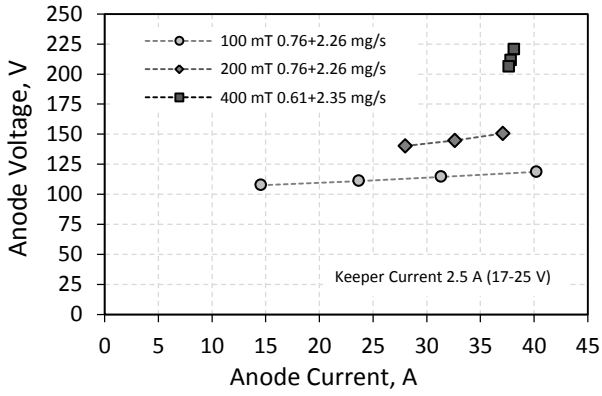

Figure 40. Anode discharge characteristic with regulated voltage operation and with keeper current of 2.5 A (heater off).

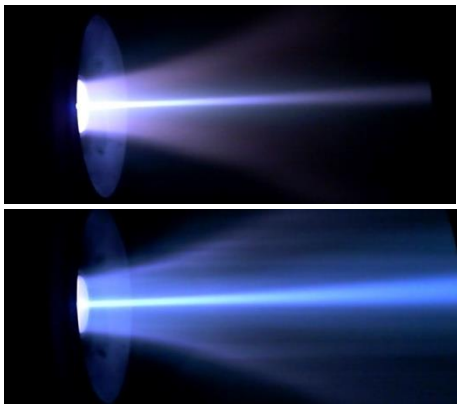

Figure 41. Plume appearance at anode voltage of 150 V, 200 mT (top), and 220 V, 400 mT (bottom), (heater off, keeper: 2.5 A).

IV. Conclusion

New thrust balance improvements and reviewed test procedures led to a significant increase of consistency and better results not only of tare forces, but also of thrust measurements compared to previous campaign in 2016.[6] The ambient pressure dependency has been characterized at different conditions, leading to the conclusion, that ambient interaction takes place via ambient gas re-entrainment and needs to be taken into account for evaluation of presented performance results.

The variation of mass flow rate distribution between cathode and anode gas shows the importance on discharge characteristics and performance. A new operation regime in high voltage mode has been identified and tested up to 240 V in regulated current operation with WT20 12/6 cathode with different plume shape appearance. Multiple conditions have been tested up to 100 kW of discharge power.

A new modular Lab_6 hollow cathode was design, manufactured and tested up to 40 A between 100 and 220 V of anode voltage in regulated voltage operation. Overall it can be concluded that AF-MPD thrusters have still enough potential for high power application. However, more research needs to be done especially in relevant vacuum conditions on more optimized thrusters, which are specifically designed for self-field centric, swirl centric or hybrid/Hall centric acceleration.

Acknowledgments

A. Boxberger thanks his wife for being so patient and his special “Arbeitskollegen” for last years at IRS.

References

[1]Löb H., Krülle G. et al.,"*Nuclear engineering for satellites and rockets*", Verlarg Karl Thiemig, Band 36, (English and German), München, 1970, Chapter IV.3, pp. 286-303.

[2]Schmidt T. D., Dachwald B., Seboldt W. and Auweter-Kurtz M., "Flight Opportunities from Mars to Earth for Piloted Missions Using Continuous Thrust Propulsion", *39th Joint Propulsion Conference*, AIAA Paper 2003-4573, 2003.

[3]Frisbee R., Hoffman N., "Electric Propulsion Options for Mars Cargo Missions", *32nd Joint Propulsion Conference and Exhibit*, AIAA Paper 1996-3173, 1996.

[4]Frisbee R., Hoffman N., "Electric Propulsion Options for Mars Cargo Missions", *32nd Joint Propulsion Conference and Exhibit*, AIAA Paper 96-3173, 1996.

[5]Gilland J., Myers R., Patterson M., "Multimegawatt Electric Propulsion System Design Considerations", *21st International Electric Propulsion Conference*, AIAA Paper 90-2552, 1990.

[6]Boxberger A., Herdrich G., "Integral Measurements of 100 kW Class Steady State Applied-Field Magnetoplasmadynamic Thruster SX3 and Perspectives of AF-MPD Technology", *35th International Electric Propulsion Conference*, IEPC Paper 2017-339, 2017.

[7]Mankar A., Boxberger A., Herdrich G., "Characterization and Improvement of Thrust Balance for High Power Applied Field MPD Thrusters", *36th International Electric Propulsion Conference*, IEPC Paper 2019-759, 2019.

[8]Kodys, A. D. and Choueiri, E. Y., "A Critical Review of the State- of-the-Art in the Performance of Applied-field Magneto-plasmadynamic Thrusters". *41st Joint Propulsion Conference & Exhibit*, AIAA Paper 2005-4247, 2005.

[9]Kruelle, G. and Zeyfang, E., "Preliminary Conclusions of Continuous Applied Field Electromagnetic Thruster Research at DFVLR", *11th Electric Propulsion Conference*, AIAA Paper 75-417, 1975.

[10]Myers R. M., "Geometric Scaling of Applied-Field Magnetoplasmadynamic Thrusters", *AIAA Journal of Propulsion and Power*, Vol. 11, No. 2, 1995.

[11]Lev D. and Choueiri E. Y., "*Scaling of Efficiency with Applied Magnetic Field in Magnetoplasmadynamic Thrusters"*, Journal of Propulsion and Power, Vol. 28, No. 3, pp. 609-616, 2012.

[12]Tikhonov V. B., Semenikhin S. A., Brophy J. R. and Polk J. E., "Performance of 130 kW MPD Thruster with an External Magnetic Field and Li as a Propellant", *27th International Electric Propulsion Conference*, IEPC Paper 1997-117, 1997.

[13]Polk J., Frisbee R., Krauthamer S., Tikhonov V., Semenikhin S., Kim V., "Technology Requirements for High-Power Lithium Lorentz Force Accelerators", *Space Technology and Applications*, 387, 1505, 1997.

[14]Bruno C., Casali D., "*Superconducting Materials Applied to Electric Propulsion Systems*", Journal of Spacecraft and Rockets, Vol. 41, No.4, pp. 671, 2004.

[15]Goebel D. M., Becatti G., Reilly S., Tilley K., "High Current Lanthanum Hexaboride Hollow Cathode for 20-200kW Hall Thrusters", *35th International Electric Propulsion Conference*, IEPC Paper 2017-303, 2017.

[16]Kojima K., Yokota S., Yamasaki, J., Yonaha M., Kimura T., Kawamata Y., Yasui M., "Plasma Diagnosis by Langmuir Probing on High Current Hollow Cathode", *31st International Symposium on Space Technology and Science*, ISTS Paper 2017-b-07, 2017.

[17]Lev D. R., Mikellides I. G., Pedrini D., Goebel D. M., Jorns B. A., McDonald M. S., "*Recent Progress in Research and Development of Hollow Cathodes for Electric Propulsion*", Review of Modern Plasma Physics, Vol.3, No.1, 2019.

[18]Sasoh A., Arakawa Y., "*Thrust Formula for Applied-Field Magnetoplasmadynamic Thrusters Derived from Energy Conservation Equation"*, Journal of Propulsion and Power, Vol. 11, No. 2, pp. 351-356, 1995.

[19]Sasoh A., Kasuga H., Nakagawa Y., Matsuba T., Ichihara D., Iwakawa A., *"Electrostatic-Magnetic-Hybrid Thrust Generation in Central-Cathode Electrostatic Thruster (CC-EST)"*, Acta Astronautica, Vol. 152, pp. 137-145, 2018.

[20]Albertoni R., Rossetti P., Paganucci F., Zuin M., Martinez E. and Cavazzana R., "Experimental Study of a 100-kW class Applied-Field MPD Thruster", *32nd International Electric Propulsion Conference*, IEPC Paper 2011-110, 2011.

[21]Connolly D. J., Bishop A. R., Seikel G. R., (1971). Tests of Permanent Magnet and Super-Conducting Magnet MPD Thrusters, NASA Technical Paper, NASA TM X-67827.

[22]Kasuga H., Mizutani K., Ichihara D., Iwakawa A., Sasoh A., Kojima K., Kimura T., Kawamata Y., Yasui M., "Ten-Ampere-Level, Direct Current Operation of Applied-Field Magnetoplasmadynamic (MPD) Thruster Using LaB6 Hollow Cathode", *35th International Electric Propulsion Conference*, IEPC Paper 2017-235, 2017.

[23]Ichihara D., Uno T., Kataoka H., Jeong J., Iwakawa A., Sasoh A., "*Ten-Ampere-Level, Applied-Field-Dominant Operation in Magnetoplasmadynamic Thrusters"*, Journal of Propulsion and Power, Vol. 33, No. 2, pp. 360-369, 2017.

[24]Boxberger A., Jüstel P., Herdrich G., "Performance of 100 kW Steady State Applied-Field MPD Thruster". *31st International Symposium on Space Technology and Science*, ISTS Paper 2017-b-24, 2017.

[25]Hall. S. J., Jorns B. A., Gallimore A. D., Kamhawi H., Haag T. W., Mackey J. A., Gilland J. H., Peterson P. Y., Baird M. J., "High-Power Performance of a 100-kW Class Nested Hall Thruster", *35th International Electric Propulsion Conference*, IEPC Paper 2017-228, 2017.

[26]Jorns B. A., Gallimore A. D., Hall S. J., Peterson P. Y., Gilland J. E., Goebel D. M., Hofer R. R., Mikellides I., "Update on the Nested Hall Thruster Subsystem for the NextSTEP XR-100 Program", *54th AIAA/SAE/ASEE Joint Propulsion Conference*, AIAA 2018-4418, 2018.

[27]Hollingsworth J.,"A Graphite Orificed Hollow Cathode for an Argon Magnetoplasmadynamic Thruster", *Bachelor Thesis*, Department of Mechanical and Aerospace Engineering, Princeton University, 2017.